THE UNIVERSITY of EDINBURGH

Edinburgh Research Explorer

Minocycline reduces microgliosis and improves subcortical white matter function in a model of cerebral vascular disease

OPEN ACCESS

GLIA

WILEY

RESEARCH ARTICLE

Minocycline reduces microgliosis and improves subcortical white matter function in a model of cerebral vascular disease

Yasmina Manso[1] | Philip R. Holland[1] | Akihiro Kitamura[1] | Stefan Szymkowiak[2] |
Jessica Duncombe[1] | Edel Hennessy[1] | James L. Searcy[1] | Martina Marangoni[1] |
Andrew D Randall[3] 🆔 | Jon T. Brown[3] | Barry W. McColl[2,4] | Karen Horsburgh[1] 🆔

[1]Centre for Neuroregeneration, University of Edinburgh, Chancellor's Building, 49 Little France Crescent, Edinburgh, EH16 4SB, United Kingdom

[2]University of Edinburgh, The Roslin Institute, Easter Bush, Edinburgh, EH25 9RG

[3]University of Exeter Medical School, University of Exeter, Exeter, UK

[4]UK Dementia Research Institute, University of Edinburgh, Edinburgh Medical School, 47 Little France Crescent, Edinburgh, EH16 4TJ, UK

Correspondence
Professor Karen Horsburgh, PhD, Centre for Neuroregeneration, The Medical School, University of Edinburgh, Chancellor's Building, 49 Little France Crescent, Edinburgh, EH16 4SB, Tel. +44(0)131 242 6216.
Email: karen.horsburgh@ed.ac.uk

Present addresses
Yasmina Manso, Developmental Neurobiology and Regeneration Lab, Parc Científic De Barcelona, Barcelona 08028 Spain 10-12 Baldiri Reixac and Philip R. Holland, Department of Basic and Clinical Neuroscience Institute of Psychiatry, Psychology and Neuroscience, King's College London, London, United Kingdom

Abstract

Chronic cerebral hypoperfusion is a key mechanism associated with white matter disruption in cerebral vascular disease and dementia. In a mouse model relevant to studying cerebral vascular disease, we have previously shown that cerebral hypoperfusion disrupts axon-glial integrity and the distribution of key paranodal and internodal proteins in subcortical myelinated axons. This disruption of myelinated axons is accompanied by increased microglia and cognitive decline. The aim of the present study was to investigate whether hypoperfusion impairs the functional integrity of white matter, its relation with axon-glial integrity and microglial number, and whether by targeting microglia these effects can be improved. We show that in response to increasing durations of hypoperfusion, the conduction velocity of myelinated fibres in the corpus callosum is progressively reduced and that paranodal and internodal axon-glial integrity is disrupted. The number of microglial cells increases in response to hypoperfusion and correlates with disrupted paranodal and internodal integrity and reduced conduction velocities. Further minocycline, a proposed anti-inflammatory and microglia inhibitor, restores white matter function related to a reduction in the number of microglia. The study suggests that microglial activation contributes to the structural and functional alterations of myelinated axons induced by cerebral hypoperfusion and that dampening microglia numbers/proliferation should be further investigated as potential therapeutic benefit in cerebral vascular disease.

KEYWORDS
blood flow, conduction velocity, microglia, minocycline, white matter integrity

1 | INTRODUCTION

Subcortical white matter is disrupted in cerebral vascular disease and dementia. Cerebral hypoperfusion is often linked with pathological changes in white matter (O'Sullivan et al., 2002) which have been detected using imaging approaches in vivo such as diffusion tensor imaging (Bastin et al., 2009; Benjamin et al., 2015; Bucur et al., 2008). Neuropathological investigations have also revealed marked alterations in white matter including reductions in myelin density in vascular disease (Barker, Wellington, Esiri, & Love, 2013; Ihara et al., 2010) with evidence that this may be related to reduced white matter perfusion (Barker et al., 2014; Fernando et al., 2006). Importantly the extent and presence of these white matter changes are now considered to be important determinants of cognitive function and influence dementia (Chen et al., 2016; Prins & Scheltens, 2015).

We and others have shown using experimental models of cerebral hypoperfusion that the brain's white matter is particularly vulnerable to modest reductions in blood flow. Specifically, reduced cerebral

perfusion elicits diffuse damage to myelinated axons accompanied by a pronounced pro-inflammatory response and impaired spatial working memory. (Coltman et al., 2011; Holland et al., 2011, 2015; McQueen, Reimer, Holland, & Horsburgh, 2014; Reimer et al., 2011; Shibata, Ohtani, Ihara, & Tomimoto, 2004) Moreover, hypoperfusion leads to the disruption of key paranodal and internodal proteins which are essential for the stability of the axon-glial connection (Reimer et al., 2011). Myelinated axons have a unique and highly organized molecular structure that enables rapid and efficient action potential propagation (Hartline and Colman, 2007). Alterations in axon-glial integrity and disruption of the protein architecture of nodal regions have been shown to impair axonal function (Boyle et al., 2001; Nie et al., 2006; Pillai et al., 2009; Ritter et al., 2013). Indeed, recent mathematical modelling indicates that subtle paranodal disruption is sufficient to significantly slow axonal conduction velocity i.e., the speed at which action potentials propagate along myelinated axons (Babbs and Shi, 2013). As yet mechanisms linking subtle reductions in blood flow to axon-glial alterations are unknown as are the impacts this has on axonal function.

Microglia are the resident immune cells of the brain and, in response to injury, secrete various factors such as cytokines and chemokines that can modulate the pathological outcome. Increased numbers of microglia often accompany damage to myelinated axons in rodent models of hypoperfusion (Coltman et al., 2011; McQueen et al., 2014; Reimer et al., 2011). Similarly increased numbers of microglia have been identified in white matter lesions in aged post-mortem human brain (Simpson et al., 2007). Activated microglia (defined by their altered morphology and increased expression of pro-inflammatory genes) predominate in the white matter of aged primate brain and correlate with cognitive impairment (Sloane, Hollander, Moss, Rosene, & Abraham, 1999). Increased numbers of activated microglia have also been linked to axon-glial disruption in an experimental model of multiple sclerosis (Howell et al., 2010). It is not clear, however, whether these changes in microglia number or phenotype contribute to, or are consequence of, the damage to myelinated axons. Potential anti-inflammatory agents or drugs that inhibit microglia, such as minocycline, can exert a protective effect on white matter structure as a consequence of hypoperfusion (Choe et al., 2006; Ma et al., 2015) and hypoperfusion/hypertension (Jalal et al., 2015). However to date it is not known whether minocycline has a protective effect on white matter function and if this is related to microglia.

The aim of the present study was to investigate whether, in response to increased durations of hypoperfusion, the functional integrity of white matter is impaired and related to axon-glial integrity and microglia numbers/proliferation. Second to this we tested the potential protective effect of minocycline on white matter function and microglia numbers/proliferation.

2 | MATERIALS AND METHODS

2.1 | Animal cohorts

All experiments were conducted under the UK Home Office Animals (Scientific Procedures) Act 1986, in agreement with local ethical and

veterinary approval (Biomedical Research Resources, University of Edinburgh) and the ARRIVE guidelines. Adult (25–30 g) male C57Bl/6J mice (Charles River Laboratories Inc, UK) were used for all experiments. At the outset, mice were coded and randomly assigned to experimental groups and investigators were blinded to the surgical or drug intervention. In Study 1, to assess temporal alterations in white matter function, mice were allocated to sham or hypoperfusion surgery to be studied at either 1, 6, or 12 weeks after surgery (12 sham and 12–13 hypoperfused mice per time-point). In Study 2, to assess the effect of minocycline treatment, mice were assigned to hypoperfusion or sham surgery and treatment with either vehicle sham ($n = 10$) or hypoperfusion vehicle ($n = 11$) or minocycline ($n = 9$). The majority of the mice had a good recovery but those that had a poor recovery were excluded from the study (study 1; 1 week $n = 3$ and 12 weeks $n = 3$ hypoperfusion; Study 2 all mice recovered well). In Study1, one animal from the 6 week cohort was excluded and in Study 2 two mice (one sham and one hypoperfusion vehicle) were excluded as electrophysiological recordings were unable to be measured. This resulted in final cohort sizes as follows: Study 1—1 week (sham $n = 12$; hypoperfusion $n = 9$); 6 weeks (sham $n = 12$; hypoperfusion $n = 12$); 12 weeks (sham $n = 12$; hypoperfusion $n = 9$). Study 2 vehicle sham ($n = 9$) or hypoperfusion vehicle ($n = 10$) or hypoperfusion minocycline ($n = 9$).

2.2 | Chronic cerebral hypoperfusion and minocycline treatment

Chronic cerebral hypoperfusion was induced by bilateral carotid artery stenosis as previously described (Coltman et al., 2011; Reimer et al., 2011). Briefly, 0.18 mm internal diameter microcoils (Sawane Spring Co, Shizuoka, Japan) were fitted on both common carotid arteries under isoflurane anaesthesia (induced at 5% and maintained at 1.2%–1.6%). A 30 minute interval was left between the placement of the first and second coil. Sham mice underwent the exact same surgical procedure with the exception that coils were not applied to the arteries. Animals were housed with free access to food and water in a 12-h dark-light cycle under constant temperature and carefully monitored throughout the experiment. Minocycline (Sigma) or vehicle was injected at a dose of 50 mg/kg,ip every other day for 10 weeks starting from day 1 after hypoperfusion surgery. This mode of drug administration was undertaken in order that we could control the dose of minocycline each mouse received. The mice habituated readily to this mode of injection. The researchers were blind to the drug administered and surgery.

2.3 | Tissue collection

At defined survival times after surgery, mice were sacrificed and their brains were quickly removed on top of a frozen petri-dish with a few drops of sucrose artificial cerebrospinal fluid, aCSF, (189 mM Sucrose, 10 mM D-glucose, 26 mM NaHCO$_3$, 3mM KCl, 5mM MgCl$_2$, 0.1 mM CaCl$_2$, 1.25mM NaH$_2$PO$_4$). The brain was then rapidly dissected, placed in a cell strainer, and submerged in ice-cold oxygenated (carbogen 95% O$_2$, 5% CO$_2$, BOC, UK) sucrose aCSF for 2–3 minutes. The brain was then glued to the cooled specimen block after carefully removing the cerebellum, transferred to the cutting chamber and

submerged in oxygenated ice-cold sucrose aCSF. Sections were then cut at 400 μm using a vibrating blade microtome (Hydrax V50, Zeiss, Cambridge, UK). A single coronal slice (in the region of −1.2 to 1.7 mm Bregma) was then transferred to a warmed (34°C) incubation chamber (BSK1, Digitimer, Welwyn Garden City, UK) with oxygenated aCSF (124 mM NaCl, 5 mM KCL, 1.25 mM NaH_2PO_4, 26 mM $NaHCO_3$, 1.3 mM $MgSO_4$, 2 mM $CaCl_2$, 10 mM D-Glucose) for one hour before electrophysiological recording. An adjacent 1.5 mm thick slice, to that of the recording slice, was cut and immediately post-fixed for 24 h in 4% paraformaldehyde, rinsed in phosphate buffer and processed for paraffin embedding.

2.4 | Electrophysiology

Recording procedures were similar to those previously published (Crawford et al., 2009). Briefly, following at least a 1 hour period of post-slicing recovery slices were carefully transferred to a recording chamber (RC27L, Harvard Apparatus, Cambridge, UK) mounted on an Olympus BX51 microscope (Olympus, KeyMed House, Southend-on-Sea, UK) where they were superfused with oxygenated aCSF (2–3 ml/min) at 24°C. This temperature was employed to enable discrimination of compound actions potentials arising from myelinated and unmyelinated fibres. Slices were supported by a slice anchor and then allowed to rest for 30 minutes prior to recording. A bipolar stimulating electrode (WPI Inc, Hertfordshire, UK) with manually blunted tips was lowered into the corpus callosum ∼1 mm lateral to the midline using a manual manipulator and constant current stimulus-isolated square wave pulses (NL800, Digitimer, Welwyn Garden City, UK) were applied to evoke compound action potentials (CAP). Recording electrodes were pulled from borosilicate glass capillaries (1.5/0.84 mm OD/ID, 100 mm long, WPI Inc., Hertfordshire, UK) and back filled with aCSF to give a final resistance of 1–3MΩ. These were connected to the amplifier's headstage via an Ag/AgCl wire and then lowered into the corpus callosum (Patchstar micromanipulator, Scientifica, East Sussex, UK) adjacent to the midline 2 mm contralateral to the stimulating electrode. For analysis of the CAP peak amplitude standardised input-output functions were generated by varying the intensity of stimulus pulse (200 μs duration, 0.2 Hz) in 0.25 mA increments from 0.25–4 mA. To enhance the signal to noise ratio, all electrophysiology analysis was conducted on averaged waveforms of four successive sweeps. Evoked CAPs were amplified (×500) and filtered (bandpass = DC to 10 kHz) using an Axopatch 200A amplifier in voltage following mode (Molecular Devices, Berkshire, UK). Responses were digitized at 200 kHz, and recorded for offline analysis using pClamp software (v10, Molecular Devices, Berkshire, UK). To assess the conduction velocity CAPs were evoked at the maximal stimulation of 4 mA and the distance between the stimulating and recording electrode altered in 0.5 mm increments from 1–2.5 mm by moving the recording electrode. The post-stimulus latency of the CAP peak was then recorded and the conduction velocity calculated based on the distance.

2.5 | Immunohistochemistry

Paraffin sections were cut at 10μm thickness. Free floating cryo-preserved sections cut at 30 μm thickness were used for the Iba-1,

TMEM119 colocalization. The antibodies used in this study were the following: $Na_{v1.6}$ (1:100, AB5580, Millipore, Nottingham, UK), Caspr (1:50, clone K65/35; UC Davies NIH NeuroMab, USA), Iba-1 (1:1000 for DAB, 1:100 for fluorescence, MP-290-CR05, Menarini, Wokingham, UK), (1:4000 for DAB, 1:500 for fluorescence, ab5076, Abcam, Cambridge, UK), Ki67 (1:25 for VIP labeling, ab16667, Abcam, Cambridge, UK), TMEM119 (1:500, ab209064, Abcam, Cambridge, UK), MAG (1:500, L20, sc-9543; Santa Cruz Biotechnology, Heidelberg, Germany). Fluorescent secondary antibodies Alexa Fluor 488, 546 and 647 (1:500) and Streptavidin Alexa Fluor 546 (1:100) were purchased from Life technologies Ltd (Loughborough, UK). Non-fluorescent biotinylated secondary antibodies were purchased from Vector Laboratories (Peterborough, UK). All sections were heat-retrieved with either EDTA pH 8 or citrate pH 6 and primary antibodies were incubated overnight at 4°C in blocking buffer (Iba-1, MAG and Caspr, MAG, Iba-1 triple label) or blocking buffer with 0.3% Triton X-100 ($Na_{v1.6}$ and Caspr double label). Sections were stained at the outset with haematoxylin and eosin to determine the presence and absence of ischemic neuronal perikaryal damage as part of the inclusion/exclusion criteria.

2.6 | Analysis of immunohistochemistry

Immunolabeled 10 μm paraffin sections were analysed using either a laser scanning confocal microscope Leica SP5 C (Milton Keynes, UK; fluorescent double and triple label) or an optical microscope Olympus BX51 (Olympus, KeyMed House, Southend-on-Sea, UK; MAG and Iba-1). Immunolabeled 30 μm free floating cryo-preserved sections immunostained with Iba-1 and TMEM119 were analyzed using a laser scanning confocal microscope Zeiss LSM710 (Zeiss, Cambridge, UK).

2.6.1 | Node-paranode measures

Images from the corpus callosum of both hemispheres (Interaural 1.98 mm; Bregma 1.82 mm according to Franklin and Paxinos, 1997) were acquired with a 63x oil-immersion objective (numerical aperture 1.4), a pinhole of 1 Airy unit and a 1024 × 1024 pixel resolution. The corresponding Nyquist settings, 4.7x zoom and 0.13 μm z-step, were used to deconvolve the image (Huygens Professional Deconvolution Software; SVI, Hilversum, The Netherlands). All length measurements were performed using ImageJ (FIJI) and the observer was blinded to the surgical procedure.

The nodal gap length, distance between paired Caspr[+] rectangular clusters, and the length of the sodium channel cluster, were measured in image stacks spanning 6 μm. The first 20 nodes that appeared in the stack and were not in contact with the borders of the image were selected for length measurements using the line tool of ImageJ. In addition, the nodal-paranodal ratio was also calculated dividing the length of the sodium channel cluster of a given node by its nodal gap length.

2.6.2 | Iba-1, Ki67, and MAG measures

The loss of axon-glial integrity of the corpus callosum was assessed using MAG immunostaining and graded from 0 (none) to 3 (extensive). Myelin damage identified with MAG was determined as the presence of disorganised white matter fibres and myelin debris. The scale was as

follows; normal (grade 0), minimal myelin debris, vacuolation, and disorganisation of fibres (grade 1), modest myelin debris, vacuolation, and disorganisation of fibres (grade 2), and extensive myelin debris, vacuolation, and disorganization of fibres (grade 3). Microglia were identified using Iba-1 and the number of positively stained cells in the corpus callosum was counted. In order to evaluate proliferation of microglia, Iba-1 was colabeled with Ki67 and the percentage of Iba-1/Ki67 cells measured within the corpus collosum.

2.6.3 | Caspr, MAG, and Iba-1 triple label imaging

Images from the corpus callosum with high and low densities of microglial cells (Interaural 1.98 mm; Bregma 1.82 mm) were acquired at different magnifications using a $40\times$ oil-immersion objective (numerical aperture 1.25) or a $100\times$ oil-immersion objective (numerical aperture 1.4), a pinhole of 1 Airy unit and a 1024×1024 pixel resolution. The corresponding Nyquist settings were used to deconvolve the images (Huygens Professional Deconvolution Software; SVI, Hilversum, The Netherlands).

2.6.4 | Iba-1, TMEM119 double labelling

Images from the corpus callosum (Interaural 1.98 mm; Bregma 1.82 mm) were acquired at $20\times$ magnification (numerical aperture 0.8), pinhole of 1–2 Airy units and a 1024×1024 pixel resolution. Images were then examined in a blinded manner for Iba-1$^+$ TMEM119$^-$ cells within the white matter.

2.7 | Real time quantitative real time polymerase chain reaction (RT-qPCR)

Corpus callosum was carefully dissected from brain slices adjacent to those used for electrophysiological analysis. RNA was extracted using a Qiagen RNeasy® midikit following manufacturer's instructions. RNA was further concentrated by precipitation. Briefly, RNA was treated with 0.3 M sodium acetate and 100% ethanol and incubated overnight at $-80°C$ to promote precipitation. Samples were then centrifuged at 15,000g for 45 min at $4°C$ and pelleted RNA resuspended in 70% ethanol and centrifugation repeated. Supernatant was then removed and samples air dried before reconstituting in RNase/DNase free water. Contaminating DNA was then removed using an Ambion® DNA-free kit following manufacturer's instructions. Complementary DNA (cDNA) was generated using superscript III reverse transcriptase. Briefly, RNA was combined with Oligo (dt)$_{15}$ (Promega, USA) and deoxynucleotide triphosphates (dNTP; Invitrogen, UK) in DNase/RNase-free water before heating to $65°C$ for 5 minutes and chilling to $4°C$ using a T100 thermal cycler. Samples were then combined with 5X first strand buffer (Invitrogen, UK), 0.1 M dithiothreitol (DTT; Invitrogen, UK), RNasin^R Plus Rnase Inhibitor (Promega, USA) and Superscript III RT (Invitrogen, UK) or RNase/DNase-free water as a control before heating to $50°C$ for 60 min and $70°C$ for 15 min using a T100 thermal cycler (BioRad, UK). For qRT-PCR analysis the following primers were designed using Primer BLAST and validated to confirm efficiency prior to use:

Arg1	Forward: 5′-GGAGACCACAGTCTGGCAGTTGGA-3′
	Reverse 5′-GGACACAGGTTGCCCATGCAGA-3′
Gapdh	**Forward 5′-TGCATCCACTGGTGCTGCCAA-3′**
	Reverse 5′-ACTTGGCAGGTTTCTCCAGGCG-3′
Il1b	Forward: 5′-CGACAAAATACCTGTGGCCTTGGGC-3′
	Reverse: 5′-TGCTTGGGATCCACACTCTCCAGC-3′
Il4rα	Forward: 5′-TCACGTGGTACAACCACTTCC-3′
	Reverse: 5′-TGCTGAAGTAACAGAACAGGCA-3′
H2-Aa	Forward 5′-CGGCTTGAACAGCCCAATG-3′
	Reverse 5′-CGCACTTTGATCTTGGCTGG-3′
Nos2	Forward 5′-GGAGACCACAGTCTGGCAGTTGGA-3′
	Reverse 5′-AGGTCGATGCACAACTGGGTGAAC-3′
Trem2	Forward 5′-CTGCTGATCACAGCCCTGTCCCAA-3′
	Reverse 5′-CCCCCAGTGCTTCAAGGCGTCATA-3′

Generated cDNA was first combined with forward and reverse primers, Platinum SYBR Green qPCR Supermix-UDG and ROX reference dye in DNase/RNase-free water. The thermal profile was then performed using a Stratagene Mx3005P thermocycler (Agilent) of the following steps: denaturation $95°C$ 10 min (1cycle); amplification, $95°C$ 15 sec, $60°C$ 20 sec, $72°C$ 1 min (40cycles); elongation $95°C$ 1 min, $55°C$ 30 sec, $95°C$ 30 sec (1 cycle). Calculated cycle threshold (Ct) values were normalised to values obtained for the housekeeping gene Gapdh and the 2$\Delta\Delta$CT method was used to determine expression fold change relative to sham control group.

2.8 | Statistical analysis

Data are presented as mean $\pm$ SEM with the exception of nodal gap and nodal-paranodal ratio data which were plotted as cumulative and relative frequency (%), respectively. Electrophysiology data and microglia counts were analysed using ANOVA and Student's unpaired t-test. Semi-qualitative MAG grading was analysed with Chi-square test for trend and nodal measures were analysed using a two-sample Kolmogorov-Smirnov test. The percentage of Iba1/Ki67 colocalised cells was compared across groups using Kruskal Wallis. Correlation analyses were done using either Pearson or Spearman test depending on parametric or non-parametric distribution of the data. Unless otherwise indicated, a probability (P) value of < 0.05 was considered to be statistically significant.

3 | RESULTS

3.1 | Functional integrity of white matter is progressively impaired in response to hypoperfusion

To test whether the functional integrity of white matter was altered in response to increased durations of hypoperfusion, extracellular CAPs were recorded in the transcallosal area of the corpus callosum. The post-stimulus latency of the CAP peak, as an index of conduction velocity, was recorded at different distances (from 1 mm to 2.5 mm from the
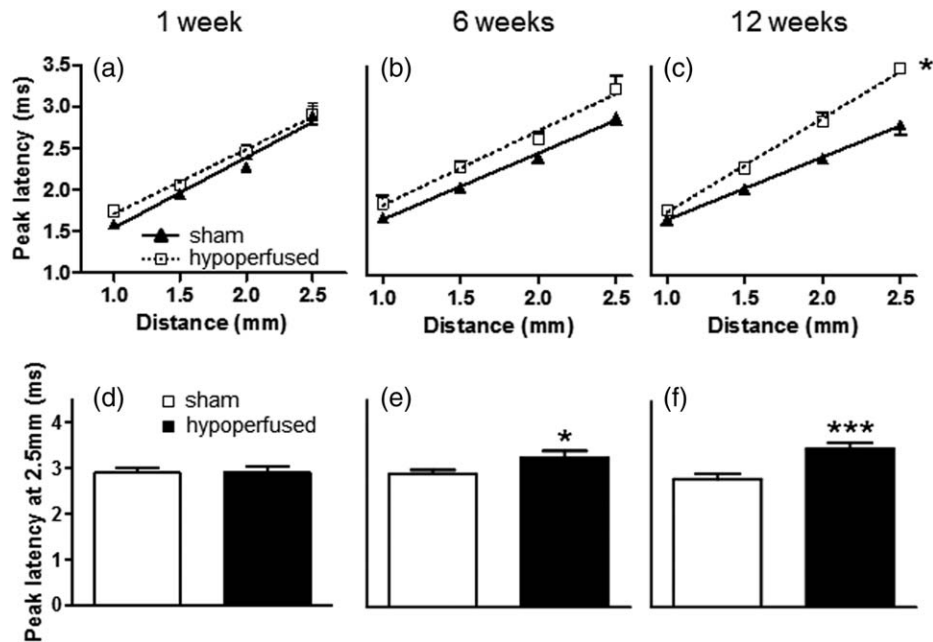
FIGURE 1 Progressive impairment of the functional integrity of myelinated axons in response to increased durations of hypoperfusion. Latency to CAP peak was progressively increased with increasing durations of hypoperfusion (a–c) indicative of impaired conduction velocity of myelinated axons. There were no significant differences following hypoperfusion at 1 week (a,d) but CAP latency was significantly increased after 6 weeks (b,e) and further at 12 weeks (c,f). Data are mean ± SEM, $n = 9$–12/group. * $P < 0.05$, ***$P < 0.001$

stimulating electrode) in the corpus callosum (Figure 1). Peak latency increased with prolonged durations of hypoperfusion (Figure 1a–c) indicative of an impaired conduction velocity in myelinated tracts. There was a significant increase in the CAP peak latency after 6 weeks ($P < 0.05$, Figure 1b,e) and 12 weeks ($P < 0.001$; Figure 1c,f) of hypoperfusion. To determine if there was any severe functional loss of white matter fibres in response to hypoperfusion the maximal peak amplitude of the CAP was compared between groups after increasing the stimulus strength from 0.25 to 4 mA. There was no significant change in the peak amplitude of myelinated fibres (data not shown) at any time-point studied indicating a lack of substantial axonal loss in our model of hypoperfusion.

3.2 | Progressive loss of paranodal and internodal axon-glial integrity in response to hypoperfusion

Our group has previously described alterations in axon-glial integrity in response to hypoperfusion (Reimer et al., 2011), associated with a disruption in the structural organisation of key proteins of the paranodal and internodal axonal domains (Figure 2a). To investigate whether the nodal-paranodal domains were altered in response to increasing durations of hypoperfusion, double-labelling of sections with antibodies against Caspr (paranodes) and Na$_{v1.6}$ (Node of Ranvier) were performed. As a measure of paranodal integrity the distance between a pair of paranodes (Caspr$^+$ clusters) from the same node (nodal gap length) was measured at 1 week, 6 weeks, and 12 weeks (Figure 2b–e). Although no alterations were detected at early time-points (1 week Figure 2f; 6 weeks Figure 2g), a significant reduction in the nodal gap length was observed after 12 weeks of hypoperfusion (Figure 2h). To examine whether alterations in the nodal-paranodal integrity could be related

with white matter function the correlation between peak latency and nodal gap length was tested. Notably there was a significant correlation between peak latency and nodal gap length in sham animals (Figure 2i; Spearman $r = -0.38$, $P < 0.05$) but no relation between peak latency and nodal gap length was determined in hypoperfused animals (Figure 2j; Spearman $r = -0.05$, $P > 0.05$) suggesting that paranodal integrity is important for proper axonal function under physiological conditions.

To explore paranodal axon-glial integrity, the nodal-paranodal ratio, which results from dividing the length of the sodium channel cluster of a given node by its nodal gap length, was calculated (Figure 3a). In normal conditions, this ratio is close to 1, since the different proteins of the axonal domains have a very distinctive and well-defined spatial distribution with limited over-lap between domains (Figure 3b). Deviations in this ratio could be indicative of loss of axon-glial integrity (Figure 3b). Consistent with our paranodal integrity results, the nodal-paranodal ratio was unchanged at early time-points (Figure 3c,d) but was significantly shifted 12 weeks after surgery (Figure 3e), indicating a loss of axon-glial integrity with increasing durations of hypoperfusion.

Internodal axon-glial integrity was further assessed using MAG immunohistochemistry in the corpus callosum. With increasing durations of hypoperfusion a progressive increase of myelin debris and vacuolation was determined (Figure 3g–i) which was absent in shams (Figure 3f). In line with paranodal data, no significant differences were found between groups at early time-points after surgery (1 week: 0.17 ± 0.39 sham vs 0.89 ± 0.60 hypoperfused $P > 0.05$; 6 weeks: 0.50 ± 0.67 sham vs 1.17 ± 1.03 hypoperfused $P > 0.05$) but there was a significant effect of hypoperfusion on axon-glial integrity 12 weeks after surgery (0.83 ± 0.72 sham vs 1.56 ± 0.88, $P < 0.05$) further supporting the disruption of axon-glial integrity in response to hypoperfusion.
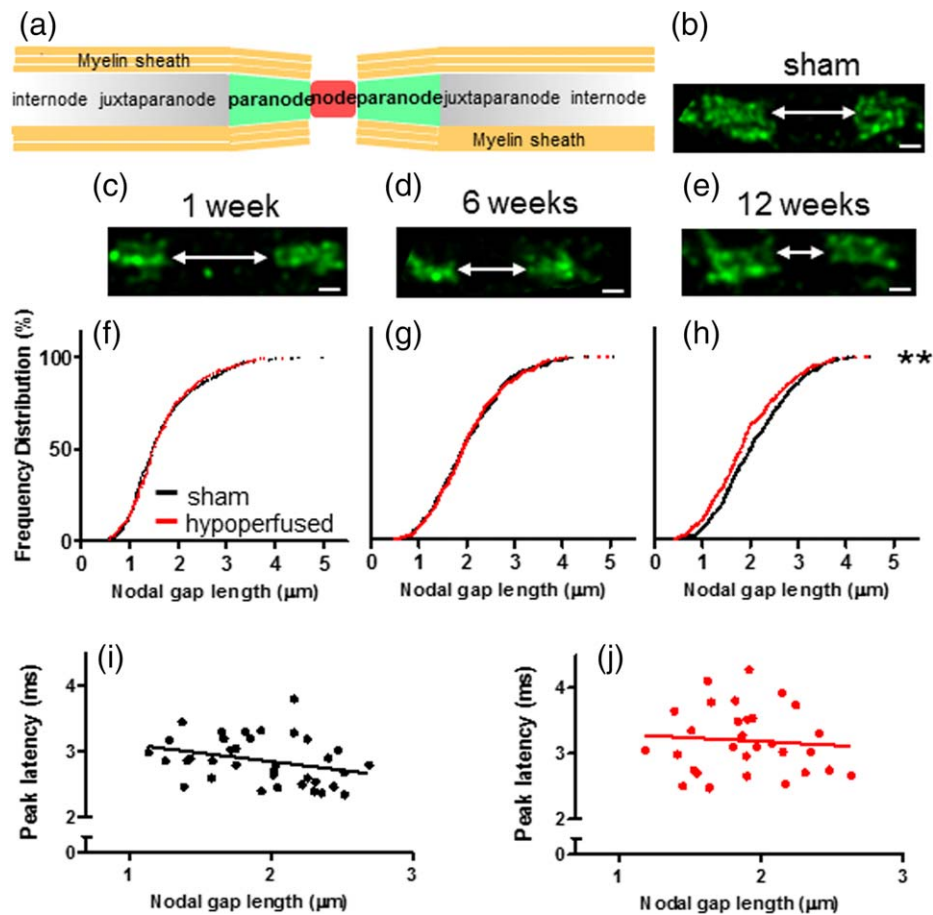
FIGURE 2 Decreased nodal gap length after hypoperfusion. Schematic representation of the axonal domains (a). The nodal gap length, i.e the distance between two paranodes of the same node, was determined using the paranodal protein Caspr (b). Forty Caspr pairs were analysed per animal (20 per hemisphere) and these 360–480 nodal gap lengths are plotted as cumulative frequency distribution (f–h). Significant reduction in the nodal gap length was observed after 12 weeks of hypoperfusion (e,h) but not at earlier time-points (c,f,d,g). There was an overall negative correlation between nodal gap length and peak latency in sham (i) but not in hypoperfused (j) mice (Spearman $r = -0.38$, $P < 0.05$; Spearman $r = -0.05$, $P > 0.05$, respectively). $n = 9$–12/group. **$P < 0.01$. Scale bar 1 μm. [Color figure can be viewed at wileyonlinelibrary.com]

3.3 | Gradual increase of microgliosis relates to impaired structural and functional integrity of white matter in response to hypoperfusion

A prominent feature of the model of cerebral hypoperfusion is a robust increase in microglia number (Coltman et al., 2011; Holland et al., 2011; McQueen et al., 2014; Reimer et al., 2011). To determine if the inflammatory response was increased in response to different durations of hypoperfusion the number of microglial cells was counted in the corpus callosum of Iba-1 stained sections (Interaural 1.74 mm; Bregma 2.06 mm). The number of Iba-1$^+$ cells gradually increased in response to prolonged durations of hypoperfusion (Figure 4a–c). As early as 1 week after hypoperfusion (Figure 4a), microglial numbers were increased compared to control. At 6 weeks and 12 weeks this increase in microglia was pronounced and significantly greater than that observed in controls ($P < 0.05$ Figure 4b,c).

It was then determined whether the increase in Iba-1 positive cells, found in the corpus callosum post-hypoperfusion, were microglia in origin or driven by macrophage infiltration. The recently developed microglia specific marker TMEM119 (Bennett et al., 2016) was colocalized with Iba-1 and quantified to delineate infiltrating macrophage cells from resident microglia. Representative images are shown of Iba-1 immunostaining in sham (Figure 4d) and hypoperfused (Figure 4h); TMEM119 immunostaining in sham (Figure 4e) and hypoperfused (Figure 4i) and then Iba-1/TMEM119 co-localisation in sham (Figure 4f,g) and hypoperfused (Figure 4j,k) white matter. All (100%) Iba-1$^+$ cells in both sham (Figure 4d) and hypoperfused cohorts (Figure 4h) were also TMEM119$^+$ (Figure 4e,i) indicating that the cells in the corpus callosum were microglia and the increase was not driven by macrophage infiltration.

To investigate whether the increase in microglial cells was associated with the loss of paranodal and axon-glial integrity, the correlations between nodal gap length and number of microglial cells, and nodal/paranodal ratio and number of microglial cells were tested. Remarkably, there was an overall negative correlation between the length of the nodal gap and the microglial counts (Figure 4l; Spearman $r = -0.55$, $P < 0.0001$), indicating that higher levels of microglia correlate with reductions in the nodal gap length (i.e. loss of paranodal integrity). In addition, there was a positive correlation between axon-glial integrity and microglial number (Figure 4m; Spearman $r = -0.37$, $P < 0.005$). To determine whether the microgliosis could also be related to the
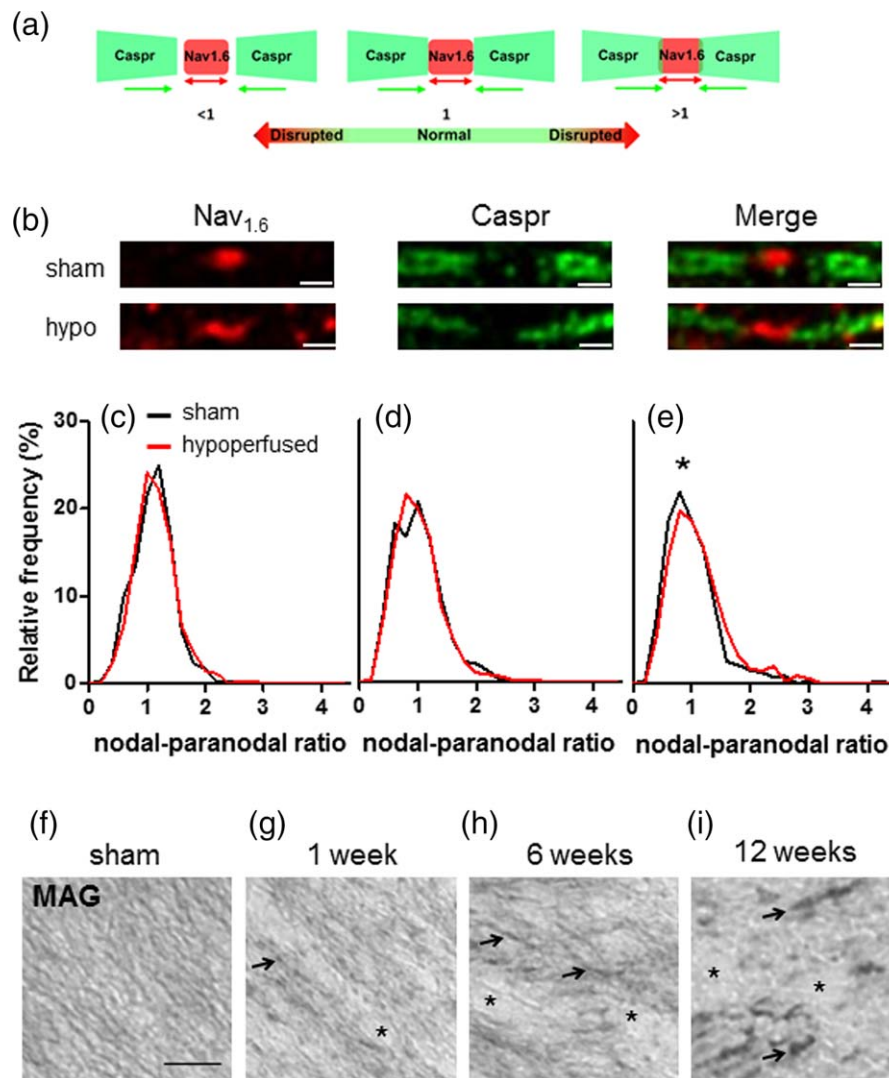
FIGURE 3 Disrupted axon-glial integrity after hypoperfusion. Schematic to indicate the nodal-paranodal ratio, which is close to 1 in intact nodes (a), and results from dividing the nodal length of a given node by its nodal gap length which is indicative of axon-glial integrity. (b) Representative images to highlight the normal spatial relationship between the node (Nav1.6) and paranodes (Caspr) in a sham and the disruption with hypoperfusion. Scale bar 1 μm. No differences in the nodal-paranodal ratio were observed after 1 (c) and 6 (d) weeks of hypoperfusion but it was significantly shifted 12 weeks after hypoperfusion (e) suggesting a loss of nodal-paranodal integrity at this time point. Ratio data is plotted as relative frequency. n=9–12/group. *p <0.05. (f–i) Representative images of myelin-associated glycoprotein (MAG) staining showing normal tissue (f) and progressive loss of axon-glia integrity in the corpus callosum with increasing durations of hypoperfusion (g–i). Myelin debris (arrow) and vacuolation (asterisk) were gradually increased after hypoperfusion compared to sham operated mice. Scale bar 25 μm. [Color figure can be viewed at wileyonlinelibrary.com]

progressive worsening of white matter function, the correlation between peak latency and the number of microglial cells was tested. Interestingly, there was an overall positive correlation between the number of microglial cells and the peak latency (Figure 4n; Spearman $r = 0.37$, $P < 0.005$), suggesting that higher levels of inflammation relate to greater deficits in the functional integrity of white matter over time.

Altogether, the results suggest that there might be a direct association between hypoperfusion-induced white matter microgliosis and disruption of paranodal and internodal integrities (Figure 5). Interestingly, it seems that areas devoid of activated microglia (Figure 5c,g) are associated with highly organised myelin fibres (Figure 5a,e) and well-preserved Caspr at paranodes (Figure 5b,f) whereas activated microglia in hypoperfusion (Figure 5k,o) are associated with disorganized myelinated tracts (Figure 5i,

m) and a loss of paranodal integrity (Figure 5j,n). Since the integrity of axonal domains is critical for efficient neuronal communication, this could ultimately impact on white matter function and cognition.

3.4 | Minocycline treatment reduces microgliosis and restores white matter functional integrity after hypoperfusion

To test whether microglia contribute to the functional impairment of white matter after hypoperfusion, we investigated the effects of minocycline. Treatment was initiated 1 day after sham or hypoperfusion surgery and lasted for 10 weeks. Notably, minocycline treatment effectively restored white matter functional integrity (Figure 6a). The
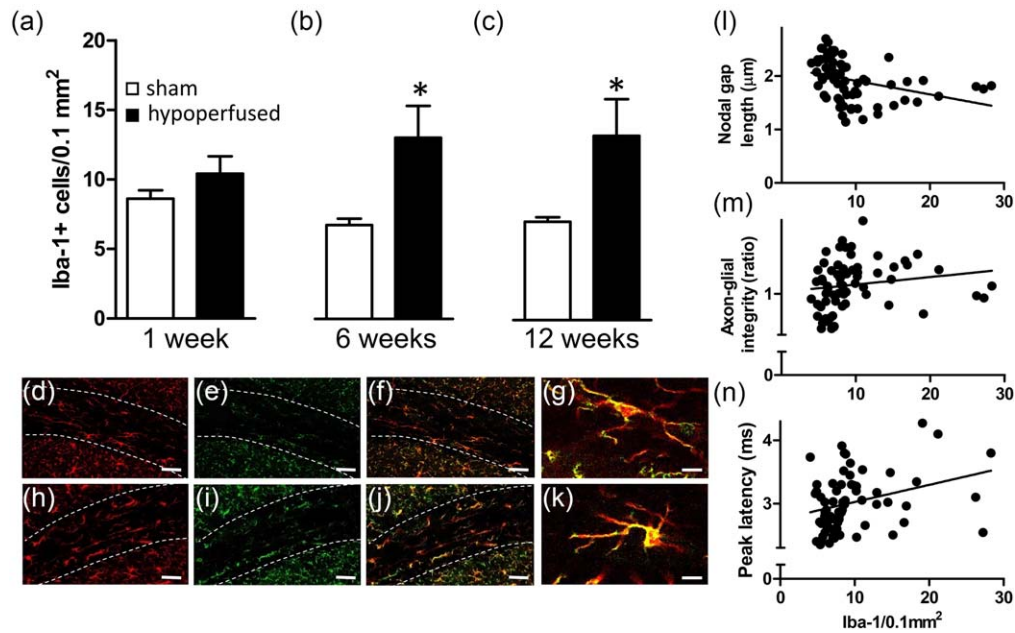
FIGURE 4   Microgliosis is increased in response to hypoperfusion and is associated with structural and functional alterations. Iba-1 labelled microglia show a progressive increase in the corpus callosum of hypoperfused mice (a-c). The number of microglial cells increased after hypoperfusion and were significantly greater at 6 (b) and 12 weeks (c) compared with sham (*$P < 0.05$). Representative images of sham (d–g) and hypoperfusion (h–k) at 12 weeks post-surgery are shown to illustrate Iba-1 immunostaining in sham (d) and hypoperfused (h); TMEM119 immunostaining in sham (e) and hypoperfused (i) and then Iba-1/TMEM119 co-localisation in sham (f,g) and hypoperfused (j,k) white matter. All Iba-1^{+} cells in both sham and hypoperfused cohorts were also TMEM119^{+} indicating that the cells in the corpus callosum were resident microglia. Scale bars; d-f and h-j are 50μm, g and k 10 μm. The number of microglial cells significantly correlated with nodal gap length (l; Spearman $r = 0.55$, $P < 0.0001$), axon-glial integrity (m; Spearman $r = 0.37$, $P < 0.005$) and CAP peak latency (n; Spearman $r = 0.37$, $P < 0.005$). Data are mean ± SEM, $n = 9$–12/group. * $P < 0.05$. [Color figure can be viewed at wileyonlinelibrary.com]
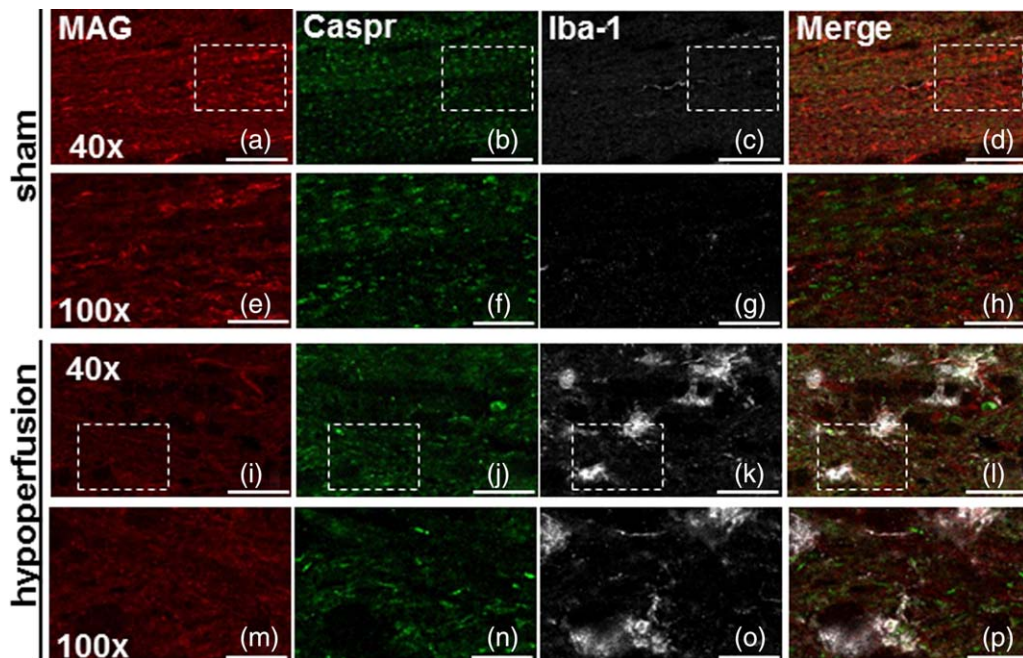

FIGURE 5   Gradual increase in microglial cells at the corpus callosum is associated with axon-glial integrity loss. Representative images (a–p) of a triple staining labelling for MAG (red), Caspr (green), and Iba-1 (white) at low (40x) and high magnification (100x). Areas devoid of activated microglia (c,g) are associated with highly organised myelin fibres (a,e) and well-preserved caspr pairs (b,f) and gradual increase in activated microglia (k,o) is associated with disorganized fibre structure (i,m) and loss of paranodal integrity (j,n). Scale bar 40 x 25 μm; scale bar 100 x 10 μm. Merged images of MAG, Caspr and Iba1 are shown (d,h,l,p). [Color figure can be viewed at wileyonlinelibrary.com]
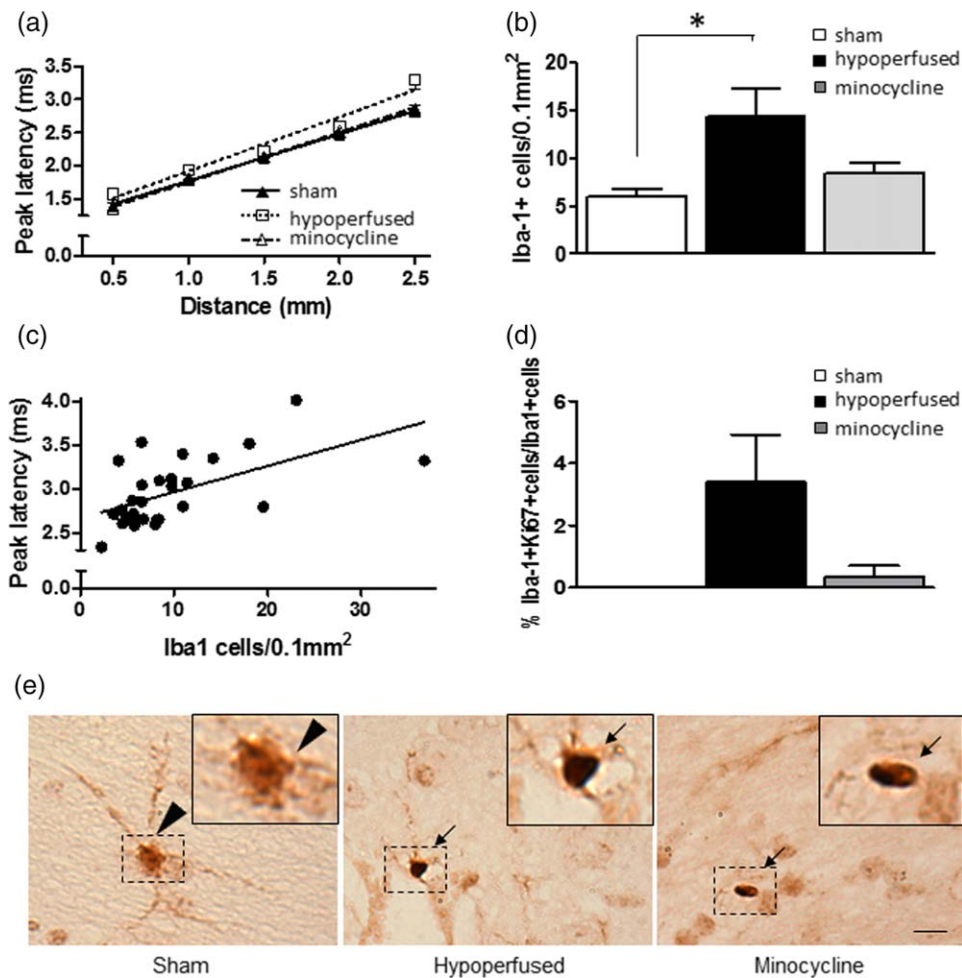
FIGURE 6 Minocycline treatment reduces microgliosis and improves white matter functional integrity. The latency to CAP of myelinated axons (a) was significantly increased after hypoperfusion and treatment with minocycline restored peak latency values to those of sham animals. Hypoperfusion significantly increased the number of microglia as compared to sham controls (b). The number of microglia in minocycline-treated hypoperfused mice were not significantly different to that of controls (b) indicating that minocycline treatment dampened the hypoperfusion-induced microgliosis. The number of microglial cells significantly correlated with peak latency (c; Pearson $r = 0.57$, $P < 0.002$) further highlighting the close association between inflammation and white matter functional integrity. There was no overall difference in the % double labelled Iba1/Ki67 cells (proliferating microglia) across the groups. Notably proliferating microglia were absent in shams and present in hypoperfused groups with fewer proliferating cells in the minocycline treated compared to vehicle treated group (d). Representative images of Iba-1 (brown) and Ki67 (black) immunolabelling; the inserts show microglia and highlights the lack of colocalisation in sham mice and presence in hypoperfused mice (e). Scale bar 10 μm Data are mean ± SEM, $n = 9$–10/group. * $P < 0.05$. [Color figure can be viewed at wileyonlinelibrary.com]

peak latency of CAPs was significantly increased in hypoperfused vehicle treated mice compared to sham vehicle treated mice ($P < 0.05$). In contrast, minocycline-treated hypoperfused mice had similar peak latencies to the sham controls ($P > 0.05$) but had significantly reduced peak latencies compared to control hypoperfused mice ($P < 0.05$). Similar to the previous study, hypoperfusion significantly increased the number of microglia as compared to sham controls ($P < 0.05$, Figure 6b). However the number of microglia in minocycline-treated hypoperfused mice were not significantly different to that of controls (Figure 6b). We next determined whether hypoperfusion influenced proliferation of microglia and if this was affected by minocycline. Iba-1 stained sections were double labelled with the proliferation marker Ki67 (see representative images Figure 6e). Overall, there was no significant difference in the % of co

localised Iba-1 immunostained cells with Ki67 ($p = 0.057$) between the groups (sham, hypoperfused vehicle, hypoperfused minocycline treated). However, it was noted that there was evidence of microglial proliferation in hypoperfused mice which was absent from sham vehicle treated mice. Further the number of proliferating microglia was reduced in minocycline treated mice as compared with hypoperfused vehicle treated mice (Figure 6d).

To further confirm whether the number of microglia could be related to white matter functional integrity, the correlation between these measures was tested. Noteworthy, and in line with our previous results, there was an overall positive correlation between the number of microglial cells and the latency to CAP peak (Figure 6c; Pearson $r = 0.57$, $P < 0.002$), indicating that increased numbers of microglia are indeed associated with a worsening of white matter function.
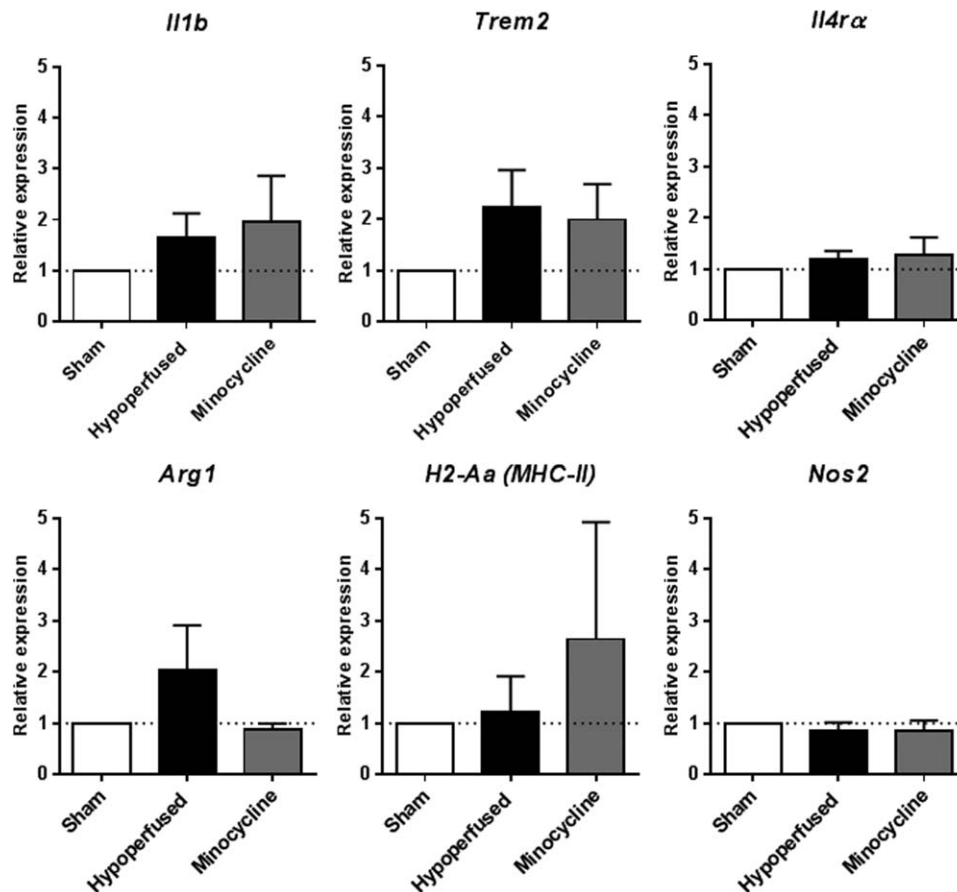
FIGURE 7 The effect of minocycline on the inflammatory profile of the corpus callosum in response to prolonged hypoperfusion. RT-qPCR analysis of gene expression in the corpus callosum following 12 weeks sham, or hypoperfusion or hypoperfusion and minocycline treatment. Cycle threshold (Ct) values of target genes were normalised to *Gapdh* and expression fold changes relative to sham group determined using $2^{\Delta\Delta Ct}$ method. Data show mean ± SEM, $n = 8–10$ per group. There were no statistical differences in gene expression between the groups

3.5 | Expression of inflammatory genes are not altered in response to hypoperfusion

To investigate the potential modulation of neuroinflammatory profile by minocycline in response to hypoperfusion the expression of selected inflammatory genes were analysed in the corpus callosum via RT-qPCR (Figure 7) from those cohorts used previously for electrophysiological and immunohistochemical analysis. Although pronounced microgliosis was observed in white matter regions in response to hypoperfusion only subtle differences in gene expression were observed suggestive of a chronic low-grade inflammatory response to hypoperfusion. Furthermore, consistent alterations in archetypal pro- or anti-inflammatory genes were not observed with minocycline treatment. Therefore, although minocycline treatment reduced microgliosis and improved white matter integrity in response to hypoperfusion the negligible effects on gene expression are consistent with the subtle underlying inflammatory response to hypoperfusion alone.

4 | DISCUSSION

Previous studies, including our own, indicated that disruption of white matter structure induced by chronic cerebral hypoperfusion (Coltman

et al., 2011; Holland et al., 2011; Reimer et al., 2011; Shibata et al., 2004) is closely linked with a robust increase in microglia number. However to date it was unclear whether these structural changes in white matter are related to a functional impairment in white matter and second to this whether increased microglia contribute to these changes. The current study demonstrates that cerebral hypoperfusion induces a progressive impairment of white matter function which is closely related to axon-glial disruption and increased numbers of resident microglia. Furthermore, minocycline, an agent that can inhibit microglia proliferation and exert anti-inflammatory properties, restores the functional impairment of white matter integrity caused by chronic cerebral hypoperfusion related to a reduction in microglia number.

The mouse model of cerebral hypoperfusion used in the current study has been well characterized by our group and others (Coltman et al., 2011; Holland et al., 2011, 2015; McQueen et al., 2014; Reimer et al., 2011; Shibata et al., 2004) and has proven informative in providing mechanistic insight to cerebral vascular disease in which cerebral hypoperfusion and white matter damage are central to the pathophysiology. The current study builds on our previous work which demonstrated the vulnerability of axon-glial domains of myelinated axons to mild cerebral hypoperfusion (Reimer et al., 2011) and now shows that these structural changes in white matter are associated with a

pronounced functional impairment of white matter connectivity. It is widely accepted that the integrity of the brain's white matter is critical in regulating efficient neuronal communication and maintaining cognitive function. Rapid saltatory conduction relies on the highly organised molecular structure of myelinated fibres into distinctive domains comprising the node of Ranvier, the paranode, the juxtaparanode and the internode (Hartline and Colman, 2007). Amongst these domains, the paranode, that flanks the node of Ranvier in myelinated axons, is a key region to maintain white matter architecture. The paranodal septate-like junction, which constitutes the major site of attachment between the glial cell and the axon, acts as an electrical and biochemical barrier between axonal domains (Buttermore, Thaxton, & Bhat, 2013) and its integrity has been proven to be fundamental for proper axonal communication. For instance, studies using knockout mice deficient for proteins key in axon-glial connection at paranodal regions such as contactin, caspr and neurofascin155 show severe reductions in nerve conduction velocity even in the absence of gross myelin or axon pathology (Bhat et al., 2001; Boyle et al., 2001; Pillai et al., 2009). Moreover, alterations in the distribution of these proteins have also been shown to have a negative impact on axon-glial integrity and axonal function (Hayashi et al., 2013; Nie et al., 2006; Ritter et al., 2013; Tanaka et al., 2009) and mathematical models indicate that even subtle paranodal disruption can significantly influence conduction velocity (Babbs and Shi, 2013). Another protein essential for axon-glial interaction is MAG which is selectively localized at the periaxonal space of internodes (Quarles, 2007). Due to its specific location, far from the oligodendrocyte cell body, MAG has been shown to be more susceptible to hypoxia-like insults than other internodal proteins such as myelin basic protein or proteolipid protein (Aboul-Enein et al., 2003; Barker et al., 2013). To date, most of the white matter functional evidence has been generated from studies in peripheral nerves and only a few of these measure white matter function in the CNS (Murcia-Belmonte et al., 2016; Ritter et al., 2013; Teigler, Komljenovic, Draguhn, Gorgas, & Just, 2009). Noteworthy, these CNS studies further support the idea that changes in axonal domains could influence axonal conduction velocity. Taken together, current literature suggests that alterations in the distribution and/or molecular architecture of these discrete domains could have a dramatic impact on axonal function. Hence, the subtle but significant alterations observed in the structural architecture of axonal domains in our mild hypoperfusion model could explain, at least in part, the deficits observed in conduction velocity. In support of this, nodal gap length measurement correlated with conduction velocity in normal healthy animals, but not in the hypoperfused ones, perhaps highlighting the importance of nodal gap integrity for proper action potential propagation.

In the present study as early as 1 week after hypoperfusion, microglia numbers increase in the corpus callosum (20% increase vs. sham) and increase further after 6 and 12 weeks after hypoperfusion. Investigation was undertaken to determine whether Iba-1 positive cells were microglial in origin or driven by macrophage infiltration. To address this we used the antibody TMEM119 recently described by the Barres group as specific for microglia and not invading monocytes (Bennett et al, 2016). Our data convincingly shows 100% overlap between Iba-1

positive cells and TMEM119 positive cells in the white matter in this model of hypoperfusion. Thus infiltrating monocytes do not appear to contribute to this pool of Iba-1 labelled cells in the corpus callosum. This increase in microglia could also be accounted for in part by local proliferation determined by an increase in Iba-1/Ki67 labelled cells after hypoperfusion. Noteworthy, the number of microglial cells was significantly associated with nodal gap length and axon-glial disruption in our study. Higher numbers of microglial cells correlated with decreased nodal gap length and increased paranodal axon-glial disruption, perhaps supporting the idea that the structural alterations observed in response to hypoperfusion could be secondary to an inflammatory response.

To test whether there was a causal relation between increased microglia and impaired white matter function after cerebral hypoperfusion we investigated the effect of minocycline. This drug, can readily penetrate the blood brain barrier, and it has been shown to improve white matter structure (Jalal et al., 2015; Yang et al., 2015a; Yrjänheikki et al., 1999). The current study provided new information to show that minocycline has beneficial effects both restoring the functional impairment induced by hypoperfusion and reducing microglia number. This study extends previous reports that have focussed on the effects of minocycline on white matter structure. Studies using experimental auto-immune encephalomyelitis mouse models and samples from multiple sclerosis individuals report an association between local microglial activation and disruption of nodal-paranodal domains in areas of normal-appearing white matter. Treatment with minocycline, reduced microgliosis and nodal/paranodal disruption albeit no functional alterations were investigated (Howell et al., 2010). Minocycline has also been effectively used in models of hypoxia-ischemia insult (Cho, La, Cho, Sung, & Kim, 2006; Jalal et al., 2015; Ma et al., 2015; Yang et al., 2015b), hyperoxia (Schmitz et al., 2014), demyelination (Skripuletz et al., 2010) and intracerebral haemorrhage (Power et al., 2003; Yan et al., 2015). In these studies, minocycline significantly reduced microgliosis and promoted neuroprotection as evidenced by the attenuation of white matter damage (Cho et al., 2006; Jalal et al., 2015; Ma et al., 2015; Schmitz et al., 2014; Skripuletz et al., 2010; Yang et al., 2015b) but a direct functional on white matter was not investigated. Our new data demonstrate minocycline has beneficial effects on white matter function. A number of mechanisms for the mode of action of minocycline have been proposed in addition to microglia inhibition and anti-inflammatory properties including effects on other cells such as oligodendrocytes (Moller et al., 2016). In the present study, the mechanism by which minocycline exerts protective effects on white matter function remains unclear. There was evidence that microglial proliferation was reduced with minocycline treatment. We also measured expression of a range of inflammatory marker genes (e.g. *Nos2, Arg1, Trem1, Trem2, Il10, H2-Aa, Il4ra*) in isolated white matter by qPCR. However we did not detect changes in response to hypoperfusion alone therefore any effects of minocycline on the inflammatory profile were not possible to determine. This was perhaps not surprising given the subtle nature of the hypoperfusion insult. However, to increase the sensitivity of detection future studies should aim to assess gene alterations in isolated microglia from the white matter. It is also important that microglia phenotype is defined in

different models and in disease since this may influence the response to drug treatment and exert different effects on disease progression. Whilst the current study would suggest that reducing microglia number in a model of cerebral hypoperfusion has beneficial effects, in other studies of severe hypoperfusion occurring after stroke, transplanted human microglial cells have been shown to exert neuroprotective effects and improve functional recovery (Narantuya et al,. 2010) whereas ablating microglia worsens injury (Lalancette-Hébert et al., 2007; Szalay et al., 2016). At the present time some caution needs to be exerted in translating these preclinical findings to drug studies in patient cohorts. It is important that microglial phenotype and broader neuroinflammatory environment at the time of drug administration is further investigated since the response may differ.

In summary, our data show that axonal function in the corpus callosum is progressively impaired in response to mild reductions of blood flow and is related to disruption of axon-glial integrity and microglial numbers. Modulation of microglial numbers and phenotype should be further investigated as potential targets for intervention in cerebral vascular disease.

REFERENCES

Aboul-Enein, F., Rauschka, H., Kornek, B., Stadelmann, C., Stefferl, A., Brück, W.,... Lassmann, H. (2003). Preferential loss of myelin-associated glycoprotein reflects hypoxia-like white matter damage in stroke and inflammatory brain diseases. *Journal of Neuropathology and Experimental Neurology*, *62*, 25–33.

Babbs, C. F., & Shi, R. (2013). Subtle paranodal injury slows impulse conduction in a mathematical model of myelinated axons. *PLoS One*, *8*, e67767-

Barker, R., Wellington, D., Esiri, M. M., & Love, S. (2013). Assessing white matter ischemic damage in dementia patients by measurement of myelin proteins. *Journal of Cerebral Blood Flow and Metabolism*, *33*, 1050-1057.

Barker, R., Ashby, E. L., Wellington, D., Barrow, V. M., Palmer, J. C., Kehoe, P. G., Esiri, M. M., & Love, S. (2014). Pathophysiology of white matter perfusion in Alzheimer's disease and vascular dementia. *Brain*, *137*, 1524-1532.

Bastin, M. E., Clayden, J. D., Pattie, A., Gerrish, I. F., Wardlaw, J. M., & Deary, I. J. (2009). Diffusion tensor and magnetization transfer MRI measurements of periventricular white matter hyperintensities in old age. *Neurobiol Aging 30*, 125-136.

Benjamin, P., Zeestraten, E. A., Lambert, C., Chis Ster, I. C., Williams, O. A., Lawrence, A. J., ... Markus, H. S. (2015). Progression of MRI markers in cerebral small vessel disease: sample size considerations for clinical trials. *Journal of Cerebral Blood Flow and Metabolism*, *3*, 1–8.

Bennett, M. L., Bennett, F. C., Liddelow, S. A., Ajami, B., Zamanian, J. L., Fernhoff, N. B., ...Barres, B. A. (2016). New tools for studying microglia in the mouse and human CNS. *Proceedings of National Academy of Sciences United States of America*, *113*, E1738-E1746.

Bhat, M. A., Rios, J. C., Lu, Y., Garcia-Fresco, G. P., Ching, W., St Martin, M., ... Bellen, H. J. (2001). Axon-glia interactions and the domain organization of myelinated axons requires neurexin IV/Caspr/Paranodin. *Neuron*, *30*, 369-383.

Boyle, M. E., Berglund, E. O., Murai, K. K., Weber, L., Peles, E., & Ranscht, B. (2001). Contactin orchestrates assembly of the septate-like junctions at the paranode in myelinated peripheral nerve. *Neuron*, *30*, 385-397.

Bucur, B., Madden, D. J., Spaniol, J., Provenzale, J. M., Cabeza, R., White, L. E., & Huettel, S. A. (2008). Age-related slowing of memory retrieval: contributions of perceptual speed and cerebral white matter integrity. *Neurobiol Aging*, 1070-1079.

Buttermore, E. D., Thaxton, C. L., & Bhat, M. A. (2013). Organization and maintenance of molecular domains in myelinated axons. *Journal of Neuroscience Research*, *91*, 603-622.

Chen, A., Akinyemi, R. O., Hase, Y., Firbank, M. J., Ndung'u, M. N., Foster, V., ... Kalaria, R. N. (2016). Frontal white matter hyperintensities, clasmatodendrosis and gliovascular abnormalities in ageing and post-stroke dementia. *Brain*, *139*, 242-258.

Cho, K.-O., La, H. O., Cho, Y. –J., Sung, K. –W., & Kim, S. Y. (2006). Minocycline attenuates white matter damage in a rat model of chronic cerebral hypoperfusion. *Journal of Neuroscience Research*, *83*, 285-291.

Coltman, R., Spain, A., Tsenkina, Y., Fowler, J. H., Smith, J., Scullion, G., ... Horsburgh, K. (2011). Selective white matter pathology induces a specific impairment in spatial working memory. *Neurobiol Aging*, *32*, 2324.e7–12.

Crawford, D. K., Mangiardi, M., & Tiwari-Woodruff, S. K. (2009). Assaying the functional effects of demyelination and remyelination: revisiting field potential recordings. *Journal of Neuroscience Methods*, *182*, 25–33.

Duan, W., Gui, L., Zhou, Z., Liu, Y., Tian, H., Chen, J. –F., Zheng, & J. (2009). Adenosine A2A receptor deficiency exacerbates white matter lesions and cognitive deficits induced by chronic cerebral hypoperfusion in mice. *Journal of Neurological Sciences*, *285*, 39–45.

Fernando, M. S., Simpson, J. E., Matthews, F., Brayne, C., Lewis, C. E., ... Ince, P. G. (2006). White matter lesions in an unselected cohort of the elderly: molecular pathology suggests origin from chronic hypoperfusion injury. *Stroke*, *37*, 1391–8.

Fu, Y., Sun, W., Shi, Y., Shi, R., & Cheng, J.-X. (2009). Glutamate excitotoxicity inflicts paranodal myelin splitting and retraction. *PLoS One*, *4*, e6705-

Hartline, D. K. & Colman, D. R. (2007). Rapid conduction and the evolution of giant axons and myelinated fibers. *Current Biology*, *17*, R29-R35.

Hayashi, A., Kaneko, N., Tomihira, C., & Baba, H. (2013). Sulfatide decrease in myelin influences formation of the paranodal axo-glial junction and conduction velocity in the sciatic nerve. *Glia*, *61*, 466-474.

Holland, C. M., Smith, E. E., Csapo, I., Gurol, M. E., Brylka, D. A., Killiany, R. J., ... Greenberg SM. (2008). Spatial distribution of white-matter hyperintensities in Alzheimer disease, cerebral amyloid angiopathy, and healthy aging. *Stroke*, *39*, 1127–33.

Holland, P. R., Bastin, M. E., Jansen, M. A., Merrifield, G. D., Coltman, R. B., Scott, F., ... Horsburgh K. (2011). MRI is a sensitive marker of subtle white matter pathology in hypoperfused mice. *Neurobiol Aging*, *32*, 2325.e1–6.

Holland, P. R., Searcy, J. L., Salvadores, N., Scullion, G., Chen, G., Lawson, G., ...Horsburgh K. (2015). Gliovascular disruption and cognitive deficits in a mouse model with features of small vessel disease. *Journal of Cerebral Blood Flow and Metabolism*, *35*, 1005–14.

Howell, O. W., Rundle, J. L., Garg, A., Komada, M., Brophy, P. J., & Reynolds, R. (2010). Activated microglia mediate axoglial disruption that

contributes to axonal injury in multiple sclerosis. *Journal of Neuropathology and Experimental Neurology*, 69, 1017–33.

Ihara, M., Polvikoski, T. M., Hall, R., Slade, J. Y., Perry, R. H., Oakley, A. E., ... Kalaria RN. (2010). Quantification of myelin loss in frontal lobe white matter in vascular dementia, Alzheimer's disease, and dementia with Lewy bodies. *Acta Neuropathology*, 119, 579–89.

Jalal, F. Y., Yang, Y., Thompson, J. F., Roitbak, T., & Rosenberg, G. A. (2015). Hypoxia-induced neuroinflammatory white-matter injury reduced by minocycline in SHR/SP. *Journal of Cerebral Blood Flow and Metabolism*, 35, 1145-1153.

Lalancette-Hébert, M., Gowing, G., Simard, A., Weng, Y. C., & Kriz, J. (2007). Selective ablation of proliferating microglial cells exacerbates ischemic injury in the brain. *Journal of Neuroscience*, 27, 2596–605.

Ma, J., Zhang, J., Hou, W. W., Wu, X. H., Liao, R. J., Chen, Y., ... Hu WW. (2015). Early treatment of minocycline alleviates white matter and cognitive impairments after chronic cerebral hypoperfusion. *Scientific Reports*, 5, 12079-

McQueen, J., Reimer, M. M., Holland, P. R., & Horsburgh, K. (2014). Restoration of oligodendrocyte pools in a mouse model of chronic cerebral hypoperfusion. *Plos One*, 9, e87227-

Möller, T., Bard, F., Bhattacharya, A., Biber, K., Campbell, B., Dale, E., ... (2016). Critical data-based re-evaluation of minocycline as a putative specific microglia inhibitor. *Glia*, 64, 1788-1794.

Murcia-Belmonte, V., Esteban, P. F., Martínez-Hernández, J, Gruart, A., Luján, R., Delgado-García, J. M., & de Castro, F. (2016). Anosmin-1 over-expression regulates oligodendrocyte precursor cell proliferation, migration and myelin sheath thickness. *Brain Structure and Function*, 221, 1365-1385.

Narantuya, D., Nagai, A., Sheikh, A. M., Masuda, J., Kobayashi, S., Yamaguchi, S., & Kim, S. U. (2010). Human microglia transplanted in rat focal ischemia brain induce neuroprotection and behavioral improvement. *PLoS One*, 5, e11746-doi: 10.1371/journal.pone.0011746.

Nie, D. -.Y, Ma, Q.-H., Law, J. W. S., Chia, C.-P., Dhingra, N. K., Shimoda, Y., ... Xiao, Z. -C. (2006). Oligodendrocytes regulate formation of nodes of Ranvier via the recognition molecule OMgp. *Neuron Glia Biology*, 2, 151-164.

O'Sullivan, M., Lythgoe, D. J., Pereira, A. C., Summers, P. E., Jarosz, J. M., Williams, S. C. R., & Markus, H. S. (2002). Patterns of cerebral blood flow reduction in patients with ischemic leukoaraiosis. *Neurology*, 59, 321-326.

Pillai, A. M., Thaxton, C., Pribisko, A. L., Cheng, J. –G., Dupree, J. L., & Bhat, M. A. (2009). Spatiotemporal ablation of myelinating glia-specific neurofascin (Nfasc NF155) in mice reveals gradual loss of paranodal axoglial junctions and concomitant disorganization of axonal domains. *Journal of Neuroscience Research*, 87, 1773-1793.

Power, C., Henry, S., Del Bigio, M. R., Larsen, P. H., Corbett, D., Imai, Y., Yong, V. W., & Peeling, J. (2003). Intracerebral hemorrhage induces macrophage activation and matrix metalloproteinases. *Annals of Neurology*, 53, 731–742.

Prins, N. D., & Scheltens, P. (2015). White matter hyperintensities, cognitive impairment and dementia: an update. *Nature Reviews Neurology*, 11, 157-165.

Quarles, R. H. (2007). Myelin-associated glycoprotein (MAG): past, present and beyond. *Journal of Neurochemistry*, 100, 1431-1448.

Reimer, M. M., McQueen, J., Searcy, L., Scullion, G., Zonta, B., Desmazieres, A., ... Horsburgh, K. (2011). Rapid disruption of axon-glial integrity in response to mild cerebral hypoperfusion. *Journal of Neuroscience*, 31, 18185-18194.

Ritter, J., Schmitz, T., Chew, L. –J., Bührer, C., Möbius, W., Zonouzi, M., & Gallo, V. (2013). Neonatal hyperoxia exposure disrupts axon-oligodendrocyte integrity in the subcortical white matter. *Journal of Neuroscience*, 33, 8990–9002.

Schmitz, T., Krabbe, G., Weikert, G., Scheuer, T., Matheus, F., Wang, Y., ...Endesfelder S. (2014). Minocycline protects the immature white matter against hyperoxia. *Experimental Neurology*, 254, 153-165.

Shibata, M., Ohtani, R., Ihara, M., & Tomimoto, H. (2004). White matter lesions and glial activation in a novel mouse model of chronic cerebral hypoperfusion. *Stroke*, 35, 2598-2603.

Simpson, J. E., Ince, P. G., Higham, C. E., Gelsthorpe, C. H., Fernando, M. S., ... Wharton, S. B. MRC Cognitive Function and Ageing Neuropathology Study Group. (2007). Microglial activation in white matter lesions and nonlesional white matter of ageing brains. *Neuropathology and Applied Neurobiology*, 33, 670–83.

Skripuletz, T., Miller, E., Moharregh-Khiabani, D., Blank, A., Pul, R., Gudi, V., ... Stangel, M. (2010). Beneficial effects of minocycline on cuprizone induced cortical demyelination. *Neurochemical Research*, 35, 1422-1433.

Sloane, J. A., Hollander, W., Moss, M. B., Rosene, D. L., & Abraham, C. R. (1999). Increased microglial activation and protein nitration in white matter of the aging monkey. *Neurobiol Aging*, 20, 395–405.

Szalay, G., Martinecz, B., Lénárt, N., Környei, Z., Orsolits, B., Judák, L., ...Dénes Á. (2016). Microglia protect against brain injury and their selective elimination dysregulates neuronal network activity after stroke. *Nature Communications*, 7, 11499-

Tanaka, H., Ma, J., Tanaka, K. F., Takao, K., Komada, M., Tanda, K., ... Ikenaka K. (2009). Mice with altered myelin proteolipid protein gene expression display cognitive deficits accompanied by abnormal neuron-glia interactions and decreased conduction velocities. *J Neurosci*, 29, 8363-8371.

Teigler, A., Komljenovic, D., Draguhn, A., Gorgas, K., & Just, W. W. (2009). Defects in myelination, paranode organization and Purkinje cell innervation in the ether lipid-deficient mouse cerebellum. *Hum Mol Genet*, 18, 1897-1908.

Yan, P., Zhu, A., Liao, F., Xiao, Q., Kraft, A. W., ... Lee, J. -M. (2015). Minocycline reduces spontaneous hemorrhage in mouse models of cerebral amyloid angiopathy. *Stroke*, 46, 1633-1640.

Yang, F., Zhou, L., Wang, D., Wang, Z., & Huang, Q. -Y. (2015a). Minocycline ameliorates hypoxia-induced blood-brain barrier damage by inhibition of HIF-1α through SIRT-3/PHD-2 degradation pathway. *Neuroscience*, 304, 250-259.

Yang, Y., Salayandia, V. M., Thompson, J. F., Yang, L. Y., Estrada, E. Y., & Yang, Y. (2015b). Attenuation of acute stroke injury in rat brain by minocycline promotes blood-brain barrier remodeling and alternative microglia/macrophage activation during recovery. *Journal of Neuroinflammation*, 12, 26-

Yrjänheikki, J., Tikka, T., Keinänen, R., Goldsteins, G., Chan, P. H., & Koistinaho, J. (1999). A tetracycline derivative, minocycline, reduces inflammation and protects against focal cerebral ischemia with a wide therapeutic window. *Proceedings of National Academy of Sciences United States of America*, 96, 13496-13500.

SUPPORTING INFORMATION

Additional Supporting Information may be found in the online version of this article.